Int. J. Appl. Math. Comput. Sci., 2002, Vol.12, No.1, 9–16

MESH r-ADAPTATION FOR UNILATERAL CONTACT PROBLEMS[†]

PIERRE BÉAL[*], JONAS KOKO[**], RACHID TOUZANI[***]

[*] NUMTECH–27, rue Jean Claret, Parc Technologique de La Pardieu,
63 063 Clermont-Ferrand Cedex 1, France,
e-mail: beal@numtech.fr

[**] Laboratoire d'Informatique, de Modélisation et d'Optimisation, des Systèmes – CNRS/FRE 2239,
Université Blaise Pascal (Clermont-Ferrand II), 63 177 Aubière Cedex, France,
e-mail: koko@isima.fr

[***] Laboratoire de Mathématiques Appliquées – CNRS/UMR 6620,
Université Blaise Pascal (Clermont-Ferrand II), 63 177 Aubière Cedex, France,
e-mail: touzani@math.univ-bclermont.fr

We present a mesh adaptation method by node movement for two-dimensional linear elasticity problems with unilateral contact. The adaptation is based on a hierarchical estimator on finite element edges and the node displacement techniques use an analogy of the mesh topology with a spring network. We show, through numerical examples, the efficiency of the present adaptation method.

Keywords: unilateral contact, linear elasticity, mesh adaptivity, node movement

1. Introduction

In contact mechanics the determination of the contact region is often a challenging issue. It generally depends on the algorithm of contact detection and its accuracy strongly depends on the mesh size. For these reasons, it seems natural to consider very fine meshes in the neighbourhood of this unknown region by making use of mesh adaptation techniques.

The aim of this paper is to present an algorithm of topology preserving mesh adaptation. It is based on a node movement rather than on mesh classical refinement/coarsening techniques. The choice of this so-called r-adaptation strategy is motivated at least by two reasons: node movement techniques preserve the matrix structure and are then well suited for large-scale computations, e.g. three-dimensional and/or nonlinear cases. Moreover, they are well adapted for differentiation with respect to node positions in order to calculate sensitivities like, for instance, in shape optimization.

The r-adaptation techniques are not new but are not popular in the numerical analysis literature. The reason for this is their lack of flexibility and their ability to generate unaesthetic meshes with a risk of degeneracy. In the present work we show that a lot of accuracy can be recovered by slightly concentrating the mesh in the regions where "something happens", e.g. in the contact region and especially in the vicinity of its boundary, where the contact pressure fails to be smooth. It turns out that in the literature one can mainly distinguish two types of r-adaptation formulations.

The first one consists in formulating the mesh adaptation problem as an energy minimization one, the optimization parameters being the solution of the boundary value problem as well as the position of mesh nodes. Clearly, this approach is possible only if the boundary value problem is equivalent to a minimization one, which is the case for frictionless contact elasticity problems. Such a method was studied in (Haslinger *et al.*, 1992), where mathematical results of existence of an optimal mesh are proved. In (Tourigny and Hülsemann, 1998), the authors give an iterative procedure to obtain an optimal mesh. The method is essentially based on a Gauss-Seidel-like method. Our tests show that although the method is attractive as it is well adapted for the problem formulation, the iterative algorithm seems to diverge in some situations, and even in the cases where it converges, edge swapping of the triangles is required. This constraint obviously alters the mesh topology. Let us note that, in addition, all optimization approaches create a difficulty related to the fact that the nondegeneracy of the triangulation must be imposed as a constraint in the problem, and that this constraint must be

[†] This work was supported by the MFP MICHELIN

satisfied at each iteration of the optimization process. This issue requires then the use of the interior penalty method, which significantly complicates the setting of the mesh adaptation problem.

In the present work, we adopt an adaptation technique based on hierarchical estimators. In other words, we use higher-order interpolation to evaluate local errors. It is noteworthy that edge-based errors are well suited for contact problems due to their ability to generate anisotropic meshes. These were introduced mainly in (D'azevedo, 1991; D'azevedo and Simpson, 1991; Habashi *et al.*, 1996). We formulate these techniques in the case of a mesh r-adaptation procedure. It turns out that, with some restrictions that will be outlined in the paper, the adaptation allows using a moderately coarse mesh with an acceptable accuracy.

The paper is organized as follows: in the next section, we present a model linear plane strain elasticity problem with Signorini's contact condition. We define a standard finite-element approximation of the problem and an iterative procedure to solve the discretized contact problem. Section 3 is devoted to the presentation of the mesh adaptation procedure. In particular, an important issue is the recovery of the hessian of the approximate solution. The mesh movement algorithm is also described. Section 4 presents some numerical tests to confirm the validity and efficiency of the method. Finally, in Section 5 some conclusions are drawn about the described method and some possible future developments.

2. Problem Statement

In this section, we recall the setting of a unilateral contact Signorini problem for linear elasticity. We consider a deformable body occupying in its reference configuration a domain Ω of $\mathbb{R}^2$ with boundary Γ divided into three disjointed subsets Γ_D, Γ_N and Γ_C. We consider furthermore a rigid obstacle described by the curve $x_2 = \phi(x_1)$. We assume that the domain, in its reference configuration, is located "above" the obstacle, i.e.

$$x_2 \geq \phi(x_1) \quad \text{for all} \quad \boldsymbol{x} = (x_1, x_2) \in \Omega.$$

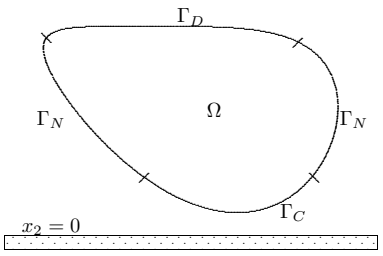

Fig. 1. A unilateral contact problem ($\phi(x_1) = 0$).

Let d denote the *contact distance* function defined by

$$d(\boldsymbol{u})(\boldsymbol{x}) := \phi(x_1) - x_2 - u_2(\boldsymbol{x}),$$

where $\boldsymbol{u}(\boldsymbol{x}) = (u_1(\boldsymbol{x}), u_2(\boldsymbol{x}))$ is the displacement of the point $\boldsymbol{x}$. The set of admissible displacements is defined by

$$\mathcal{V} := \{\boldsymbol{v} \in H^1(\Omega; \mathbb{R}^2);\ \boldsymbol{v} = 0 \text{ on } \Gamma_D,\ d(\boldsymbol{v}) \leq 0 \text{ on } \Gamma_C\},$$

where $H^1(\Omega; \mathbb{R}^2)$ is the space of vector valued functions $\boldsymbol{v}$ such that

$$\int_\Omega \left(|\boldsymbol{v}|^2 + \left| \frac{\partial \boldsymbol{v}}{\partial x_1} \right|^2 + \left| \frac{\partial \boldsymbol{v}}{\partial x_2} \right|^2 \right) \mathrm{d}\boldsymbol{x} < +\infty.$$

Here, we have placed the deformed domain above the obstacle. Moreover, we have imposed a Dirichlet boundary condition on Γ_D and a traction free boundary condition on Γ_N. We assume furthermore that the boundary Γ_D does not interact with the obstacle in the deformed configuration. The energy functional is given by

$$\mathrm{W}:\ \boldsymbol{v} \in \mathcal{V} \mapsto W(\boldsymbol{v}) = \frac{1}{2} a(\boldsymbol{v}, \boldsymbol{v}) - \int_\Omega \boldsymbol{f} \cdot \boldsymbol{v}\, \mathrm{d}\boldsymbol{x} - \int_{\Gamma_N} \boldsymbol{g} \cdot \boldsymbol{v}\, \mathrm{d}s \in \mathbb{R},$$

where a is the bilinear symmetric form defined by the linear elasticity problem. Namely,

$$a(\boldsymbol{u}, \boldsymbol{v}) = \sum_{i,j,k,l=1}^{2} \int_\Omega c_{ijkl} \varepsilon_{ij}(\boldsymbol{u}) \varepsilon_{ij}(\boldsymbol{v})\, \mathrm{d}\boldsymbol{x}, \qquad (1)$$

and $\boldsymbol{f}$ (resp. $\boldsymbol{g}$) is a smooth function that stands for the applied body (resp. boundary) force. In (1), (c_{ijkl}) is the tensor of elastic coefficients and

$$\varepsilon_{ij}(\boldsymbol{u}) = \frac{1}{2} \left(\frac{\partial u_i}{\partial x_j} + \frac{\partial u_j}{\partial x_i} \right), \quad 1 \leq i, j \leq 2$$

is the symmetric tensor of infinitesimal deformations. We choose here the case of an isotropic and homogeneous material, i.e. (c_{ijkl}) is given by

$$c_{ijkl} = \mu(\delta_{ik}\delta_{jl} + \delta_{il}\delta_{jk}) + \lambda \delta_{ij}\delta_{kl}, \quad 1 \leq i, j, k, l \leq 2,$$

the real numbers $\lambda \geq 0$ and $\mu > 0$ denoting the Lamé coefficients of the material, and δ_{ij} being the Kronecker delta. These coefficients are related in plane deformations to the Young modulus E and Poisson coefficient ν by the relationships

$$\lambda = \frac{\nu E}{(1+\nu)(1-2\nu)}, \quad \mu = \frac{E}{2(1+\nu)}.$$

The equilibrium problem consists in seeking a minimum of the functional W:

$$\text{Find } \boldsymbol{u} \in \mathcal{V} \text{ such that } W(\boldsymbol{u}) \leq W(\boldsymbol{v}) \text{ for all } \boldsymbol{v} \in \mathcal{V}. \quad (2)$$

It is well known (Kikuchi and Oden, 1988) that the solution to Problem (2) satisfies the variational inequality

$$\begin{cases} \boldsymbol{u} \in \mathcal{V}, \\ a(\boldsymbol{u}, \boldsymbol{v}-\boldsymbol{u}) \geq \displaystyle\int_\Omega \boldsymbol{f}\cdot(\boldsymbol{v}-\boldsymbol{u})\,\mathrm{d}\boldsymbol{x} \\ \qquad\qquad + \displaystyle\int_{\Gamma_N} \boldsymbol{g}\cdot(\boldsymbol{v}-\boldsymbol{u})\,\mathrm{d}s \ \text{ for all } \ \boldsymbol{v}\in\mathcal{V}. \end{cases}$$

2.1. Discrete Problem

Let us consider now a finite element approximation of Problem (2). We assume that the domain Ω is polygonal and we consider a triangulation $\mathcal{K}^h$ of Ω into triangles of diameters $\leq h$. We define the space

$$\mathcal{X}^h = \big\{\boldsymbol{v}\in\mathcal{C}^0\big(\overline{\Omega};\mathbb{R}^2\big);\ \boldsymbol{v}_{|K}\in(P_1)^2 \\ \text{for all } K\in\mathcal{K}^h,\ \boldsymbol{v}=0 \text{ on } \Gamma_D\big\},$$

where P_1 is the space of affine polynomials. Let $(\boldsymbol{a}^i)_{1\leq i\leq I}$ denote the set of nodes on Γ_C. We define furthermore, for $\boldsymbol{v}\in\mathcal{X}^h$, the contact distance at nodes $\boldsymbol{a}^i$ of Γ_C by $d_i(\boldsymbol{u}) := d(\boldsymbol{u})(\boldsymbol{a}^i)$, $1\leq i\leq I$. We also define the set

$$\mathcal{V}^h := \big\{\boldsymbol{v}\in\mathcal{X}^h;\ d_i(\boldsymbol{v})\leq 0,\ 1\leq i\leq I\big\}.$$

Notice that here, the set $\mathcal{V}^h$ is not included in $\mathcal{V}$. This feature is at the origin of some numerical difficulties in contact problems.

For each function $\boldsymbol{v}\in\mathcal{X}^h$, we define a function $d^h(\boldsymbol{v})$ on Γ_C, which is continuous, piecewise linear and which coincides with $d_i(\boldsymbol{v})$ at node $\boldsymbol{a}^i$, for all $i\in\{1,\ldots,I\}$. The discrete problem is defined by

$$\text{Find } \boldsymbol{u}^h\in\mathcal{V}^h \text{ such that} \\ W(\boldsymbol{u}^h)\leq W(\boldsymbol{v}) \text{ for all } \boldsymbol{v}\in\mathcal{V}^h. \tag{3}$$

2.2. Penalty Solution Method

In order to solve the constrained optimization problem (3), we use a standard external penalty method. For this, we define for $\varepsilon>0$ the penalized energy functional

$$W_\varepsilon(\boldsymbol{v}) := W(\boldsymbol{v}) + \frac{1}{2\varepsilon}\int_{\Gamma_C}(d^h(\boldsymbol{v})^+)^2\,\mathrm{d}s.$$

The penalized problem is defined by:

$$\text{Find } \boldsymbol{u}^h\in\mathcal{X}^h \text{ such that} \\ W_\varepsilon(\boldsymbol{u}^h)\leq W_\varepsilon(\boldsymbol{v}) \text{ for all } \boldsymbol{v}\in\mathcal{X}^h. \tag{4}$$

It is well known and easy to prove that the unique solution to Problem (4) converges, in the energy norm, to the solution to Problem (3) as $\varepsilon\to 0$.

Here, the principal interest of the penalized problem (4) is that the nonpenetration constraint is removed. It can be also shown that the solution to Problem (4) solves the variational problem

$$\begin{cases} \boldsymbol{u}^h\in\mathcal{X}^h, \\ a(\boldsymbol{u}^h,\boldsymbol{v}) + \dfrac{1}{\varepsilon}\displaystyle\int_{\Gamma_C} d^h(\boldsymbol{u}^h)^+ v_2\,\mathrm{d}s \\ \qquad = \displaystyle\int_\Omega \boldsymbol{f}\cdot\boldsymbol{v}\,\mathrm{d}\boldsymbol{x} + \int_{\Gamma_N}\boldsymbol{g}\cdot\boldsymbol{v}\,\mathrm{d}s \ \text{ for all } \boldsymbol{v}\in\mathcal{X}^h. \end{cases} \tag{5}$$

The obtained problem is thus a nonlinear one due to the nonlinearity of the boundary integral in the variational formulation (5). It remains then to build an iterative scheme to solve the nonlinearity.

2.3. Iterative Procedure

In order to solve the nonlinear problem (5), we consider the following simple iterative scheme:

$$\begin{cases} \text{Given } (\boldsymbol{u}^h)^n\in\mathcal{X}^h, \\ \text{Find } (\boldsymbol{u}^h)^{n+1}\in\mathcal{X}^h \text{ such that} \\ a\big((\boldsymbol{u}^h)^{n+1},\boldsymbol{v}\big) + \dfrac{1}{\varepsilon}\displaystyle\int_{\Gamma_C}\alpha^n d^h\big((\boldsymbol{u}^h)^{n+1}\big)v_2\,\mathrm{d}s \\ \qquad = \displaystyle\int_\Omega \boldsymbol{f}\cdot\boldsymbol{v}\,\mathrm{d}\boldsymbol{x} + \int_{\Gamma_N}\boldsymbol{g}\cdot\boldsymbol{v}\,\mathrm{d}s \ \text{ for all } \boldsymbol{v}\in\mathcal{X}^h, \end{cases}$$

for $n=0,1,2,\ldots$, where

$$\alpha^n = \begin{cases} 1 & \text{if } d^h((\boldsymbol{u}^h)^n)>0, \\ 0 & \text{otherwise.} \end{cases}$$

Hence the iterative procedure consists, for each iteration step, in detecting contact for each node by using displacements at the previous iteration.

Numerical experiments have shown good properties of this iteration process: in all cases convergence is achieved in some iterations.

Remark 1. Although the penalty term involves integrals of polynomials of degree 2, we use the trapezoidal rule to evaluate it in order to avoid well-known numerical locking.

3. Mesh r-Adaptation

Let us define our r-adaptation method. It uses, like most of mesh adaptation algorithms, an *a posteriori* error estimator. The estimator here is said to be hierarchical in the sense that it is based on a P_2-approximation of the solution. The presented method was developed by Peraire *et al.*, (1992), Habashi *et al.*, (1996), D'azevedo and Simpson, (1991), and Fortin, (1998). It is often used for an h-adaptation method, i.e. adaptation by mesh refinement of coarsening. We use it here for an r-adaptation.

Let us present the method as briefly as possible, since the details can be found in the papers (D'azevedo and Simpson, 1991; Fortin, 1998; Habashi *et al.*, 1996; Peraire *et al.*, 1992). Consider a triangle K and a polynomial $\widetilde{u}^h$ of degree 2 on K. In practice, $\widetilde{u}^h$ will stand for the restriction to K of a piecewise P_2 approximation of the solution to the problem. We consider furthermore the P_1-interpolate of $\widetilde{u}^h$, denoted by u^h. Let $e^h = \widetilde{u}^h - u^h$. It can be shown (D'azevedo and Simpson, 1991) that the error function e is proportional to the hessian $\boldsymbol{H}$ of $\widetilde{u}^h$. Using this property, we adopt the following adaptation criterion: We seek a mesh that achieves an equidistribution of the error e^h on the edges of the triangulation. Therefore, if E is an edge of the triangulation and if $\boldsymbol{\tau}_E$ is the unit tangent to E, the second derivative along the $\boldsymbol{\tau}_E$-direction is given by

$$\frac{\partial^2 \boldsymbol{u}}{\partial \boldsymbol{\tau}_E^2} = \boldsymbol{\tau}_E^T \boldsymbol{H} \boldsymbol{\tau}_E.$$

Let $\boldsymbol{x}_k$ and $\boldsymbol{x}_\ell$ denote the two vertices of the edge E. If the (constant) matrix $\boldsymbol{H}$ is semi-positive definite, we define the error estimator on E by

$$e_{k\ell} = (\boldsymbol{a}_{k\ell}^T \boldsymbol{H} \boldsymbol{a}_{k\ell})^{\frac{1}{2}}.$$

Note that, in the case where $\boldsymbol{H}$ is positive definite, this error defines a new metric on the edge E. In this case, error equidistribution on the edges is equivalent to prescribing that all the edges have the same length in the metric associated to $\boldsymbol{H}$.

3.1. Practical Computation of the Estimator

The calculation of the error $e_{k\ell}$ can be achieved in the following way: if $\boldsymbol{g}$ is the gradient of $\widetilde{u}^h$ and if we note that this one is an affine vector on the edge E, we have

$$\boldsymbol{H}\boldsymbol{a} = \begin{pmatrix} \boldsymbol{a}_{k\ell}^T \dfrac{\partial \boldsymbol{g}}{\partial x_1} \\ \boldsymbol{a}_{k\ell}^T \dfrac{\partial \boldsymbol{g}}{\partial x_2} \end{pmatrix} = \frac{\partial \boldsymbol{g}}{\partial \boldsymbol{a}_{k\ell}} = \boldsymbol{g}_k - \boldsymbol{g}_{k\ell},$$

where $\boldsymbol{g}_k = \boldsymbol{g}(\boldsymbol{x}_k)$.

When the matrix $\boldsymbol{H}$ is not semi-positive definite, we consider (as in (Fortin, 1998)) the spectral decomposition of $\boldsymbol{H}$:

$$\boldsymbol{H} = \boldsymbol{R}^T \boldsymbol{\Lambda} \boldsymbol{R},$$

where $\boldsymbol{\Lambda}$ is the diagonal matrix of the eigenvalues of $\boldsymbol{H}$. Let us denote by $|\boldsymbol{\Lambda}|$ the matrix obtained from $\boldsymbol{\Lambda}$ by replacing the eigenvalues with their absolute values and with $|\boldsymbol{H}|$ the matrix

$$|\boldsymbol{H}| = \boldsymbol{R}^T |\boldsymbol{\Lambda}| \boldsymbol{R}.$$

Using the inequality

$$|\boldsymbol{b}^T \boldsymbol{H} \boldsymbol{b}| \leq \boldsymbol{b}^T |\boldsymbol{H}| \boldsymbol{b} \text{ for all } \boldsymbol{b} \in \mathbb{R}^2,$$

we replace the hessian matrix $\boldsymbol{H}$ with $|\boldsymbol{H}|$. We now want to calculate the error

$$e_{k\ell} = \left(\boldsymbol{a}_{k\ell}^T |\boldsymbol{H}| \boldsymbol{a}_{k\ell}\right)^{\frac{1}{2}}$$

using $\widetilde{u}^h$. If $\widehat{\boldsymbol{a}}_{ij} = \boldsymbol{R}\boldsymbol{a}_{ij}$ and $\widehat{\boldsymbol{g}} = \boldsymbol{R}\boldsymbol{g}$, we have

$$\begin{aligned} \boldsymbol{a}_{k\ell}^T |\boldsymbol{H}| \boldsymbol{a}_{k\ell} &= \boldsymbol{a}_{k\ell}^T \boldsymbol{R}^T |\boldsymbol{\Lambda}| \boldsymbol{a}_{k\ell} \\ &= \boldsymbol{a}_{k\ell}^T \boldsymbol{R}^T (|\widehat{\boldsymbol{g}}_k| - |\widehat{\boldsymbol{g}}_\ell|) \\ &= \boldsymbol{a}_{k\ell}^T \boldsymbol{R}^T (|\boldsymbol{R}\boldsymbol{g}_k| - |\boldsymbol{R}\boldsymbol{g}_\ell|). \end{aligned} \tag{6}$$

It remains now to calculate the hessian. The difficulty lies in the fact that, since the approximate solution u^h is only continuous, its second partial derivatives are Dirac distributions on element edges. To approximate these distributions, we proceed as follows: A continuous approximation of the hessian matrix entries is obtained by the following projection:

$$H_{ij}(\boldsymbol{x}_k) \approx \frac{\displaystyle\int_{\Omega_k} \frac{\partial^2 u^h}{\partial x_i \partial x_j} \phi_k \, \mathrm{d}\boldsymbol{x}}{\displaystyle\int_{\Omega_k} \phi_k \, \mathrm{d}\boldsymbol{x}}, \tag{7}$$

where ϕ_k is the basis function associated with node $\boldsymbol{x}_k$ and Ω_k is the union of triangles that share this node. Let us point out that the above integrals are actually duality brackets since, as has previously been mentioned, the second-order derivatives of the approximate solution are only distributions. Effective calculation of the above expression is then obtained with the use of Green's formula:

$$H_{ij}(\boldsymbol{x}_k) \approx \frac{\displaystyle\int_{\Gamma_k} \frac{\partial u^h}{\partial x_i} \phi_k n_j \, \mathrm{d}s - \int_{\Omega_k} \frac{\partial u^h}{\partial x_i} \frac{\partial \phi_k}{\partial x_j} \, \mathrm{d}\boldsymbol{x}}{\displaystyle\int_{\Omega_k} \phi_k \, \mathrm{d}\boldsymbol{x}},$$

where Γ_k is the union of boundaries of triangles of Ω_k, and $\boldsymbol{n} = (n_i)$ is the outward unit normal to the edges Γ_k.

3.2. Node Displacement Procedure

Let us now define an algorithm to move the nodes according to the computed edge errors. For this we adopte a classical technique that considers the finite-element mesh as a network of elastic springs with stiffness coefficients that depend on the error estimator on each edge (cf. Habashi *et al.*, 1996). In this technique, node positions are interpreted as the solution of an energy minimization problem. Hooke's law for this spring network is given by

$$\sum_{\ell=1}^{n}(\boldsymbol{x}_\ell - \boldsymbol{x})\kappa_\ell(\boldsymbol{x}) = 0, \tag{8}$$

where $\kappa_\ell(\boldsymbol{x})$ is the constant of the spring with ends $\boldsymbol{x}$ and $\boldsymbol{x}_\ell$. Its dependency on the estimator is empirically chosen as

$$\kappa_\ell(\boldsymbol{x}) = \frac{e_\ell(\boldsymbol{x})}{\|\boldsymbol{x}_\ell - \boldsymbol{x}\|},$$

where $e_\ell(\boldsymbol{x})$ is the metric of the edge of vertices $\boldsymbol{x}$ and $\boldsymbol{x}_\ell$; in particular, $e_\ell(\boldsymbol{x}_k) = \boldsymbol{a}_{k\ell} = \boldsymbol{x}_k - \boldsymbol{x}_\ell$. In order to solve the nonlinear equation (8), we use a relaxation procedure, i.e. we update node positions by the iterative procedure

$$\boldsymbol{x}^{p+1} = \boldsymbol{x}^p + \omega\,\frac{\displaystyle\sum_{\ell=1}^{n}(\boldsymbol{x}_\ell - \boldsymbol{x}^p)\kappa_\ell(\boldsymbol{x}^p)}{\displaystyle\sum_{\ell=1}^{n}\kappa_\ell(\boldsymbol{x}^p)}, \quad p = 0, 1, \ldots,$$

where ω is the relaxation parameter. In practice, we do not iterate until complete convergence, i.e. we iterate until an acceptable discrepancy (say, 10^{-3}) is obtained.

Remark 2. The case of boundary nodes is treated separately. Here we project the computed new position of each boundary node on the actual boundary. Let us note that another difficulty is related to the fact that boundary nodes define the actual boundary of the domain. Any displacement of these nodes hence modifies this boundary.

3.3. Remarks

1. Numerical experiments with this method show that it is *a priori* valid only for structured meshes, i.e. meshes with a constant node connectivity. This difficulty can be explained by the fact that error equidistribution on the edges does not coincide with energy minimization of the spring network in the unstructured case. Numerical tests have shown poor behaviour in the unstructured case.

2. In practice, the convergence of the iteration process depends on the relaxation parameter ω. Obviously, a small value of ω ensures convergence with, however, a large number of iterations. Moreover, a limitation on the node displacements must be included in the procedure in order to prevent elements from degeneracy. This constraint is simply implemented by prescribing relative upper and lower bounds on edge lengths.

3.4. Numerical Tests

In order to validate the previously described adaptation method, we first present a simple test on an explicitly given function and then give two elasticity contact problems.

3.4.1. Validation Test

Consider the domain $\Omega = (0,1) \times (0,1)$ of $\mathbb{R}^2$. We construct a uniform mesh by dividing each edge of Ω into 10×10 sub-intervals. The adaptation of this mesh for the function

$$f(\boldsymbol{x}) = e^{-10\,x_1 + x_2}$$

is given in Fig. 2. The number of iterations was 51 for a value of $\omega = 0.8$.

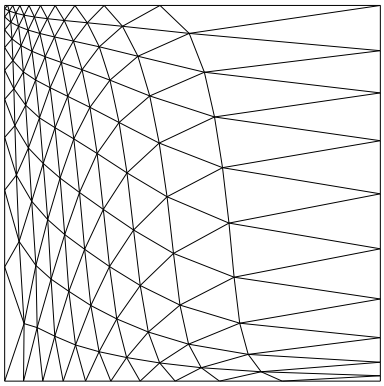

Fig. 2. Adapted mesh (case P_1).

We have also tested the behaviour of the node movement procedure when using quadrilateral Q_1 elements, and the obtained mesh is plotted in Fig. 3. We note here that the orthogonality of the mesh is preserved after adaptation. This is due to the separation of variables in the tested function f. For this example, the number of iterations was 49 for a value of $\omega = 0.8$.

3.4.2. Cantilever Beam

We consider a cantilever beam defined by the domain $\Omega = (0,4) \times (0.05,1)$ clamped at its end $x_1 = 0$ and submitted at its top side $x_2 = 1$ to a normal traction p. The beam is furthermore in potential contact with a rigid horizontal obstacle defined by the line $x_2 = 0$. We choose the data

$$p = -100, \quad E = 2\,000, \quad \nu = 0.3.$$

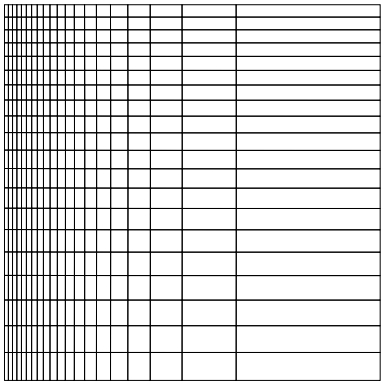

Fig. 3. Adapted mesh (case Q_1).

Figure 4 presents a uniform coarse mesh of the beam. The adaptation algorithm produces the mesh plotted in Fig. 5.

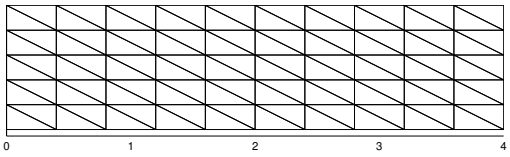

Fig. 4. Cantilever beam: Uniform mesh.

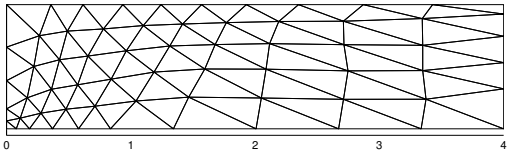

Fig. 5. Cantilever beam: Adapted mesh.

We have compared the contact pressure at the bottom $x_2 = 0$ with the one obtained with the coarse mesh (Fig. 6) and with a fine mesh (320 triangles). Figure 5 shows that, on the one hand, the mesh is displaced in the neighbourhood of the boundary of the contact region. On the other hand, the contact pressure is, as has been expected, more accurate for the adapted mesh than for the initial one.

3.4.3. Hertz Test

A classical test in the numerical simulation of contact mechanics is the Hertz contact problem. Let us recall that this one pertains to a disc in contact with a horizontal obstacle. The disc is submitted along its radius to a uniform pressure f. The details can be found, for example, in (Kikuchi and Oden, 1988). It is shown that if the radius is "large enough", then the half width of the contact region is given by

$$b = 2\sqrt{\frac{fR(1-\nu^2)}{\pi E}}$$

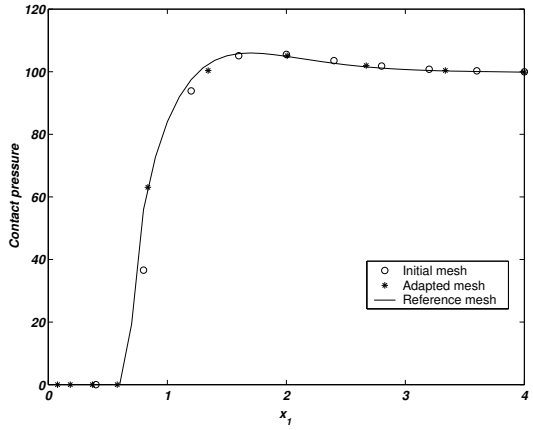

Fig. 6. Cantilever beam: Comparison of contact pressures.

and the contact pressure is given by

$$p(\boldsymbol{x}) = \frac{2f}{\pi b^2}\sqrt{b^2 - x_1^2}, \quad \boldsymbol{x} \in \Gamma_C.$$

Computations are carried out using a half disc with radius $R = 8$. Figure 7 illustrates the initial mesh of the domain in its reference configuration, while Figs. 8 and 9 illustrate the adapted mesh in the reference and deformed configurations, respectively. We can note that the adaptation process has refined the mesh in the contact region and particularly on the boundary of this region, where the contact pressure admits a discontinuity of the gradient. This was clearly the main goal of the present study.

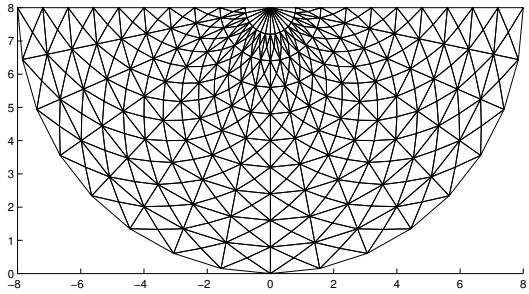

Fig. 7. Hertz test: Initial mesh.

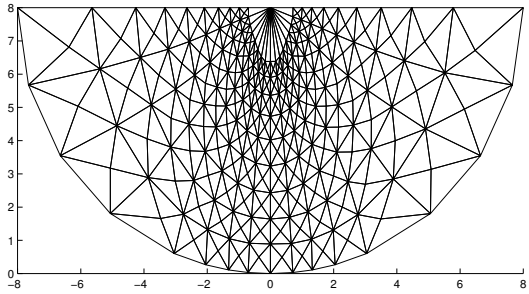

Fig. 8. Hertz test: Adapted mesh.

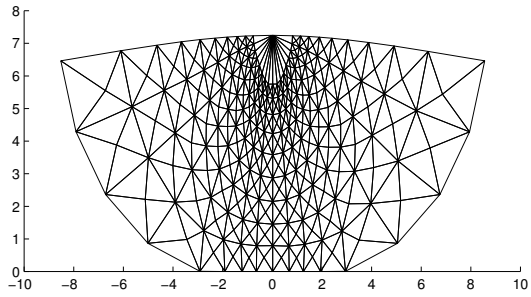

Fig. 9. Hertz test: Adapted mesh (Deformed configuration).

The efficiency of the method appears more clearly when one considers the calculated contact pressures and the determination of the contact region (Fig. 10). This one is numerically identified as the set of nodes where the boundary traction is not vanishing.

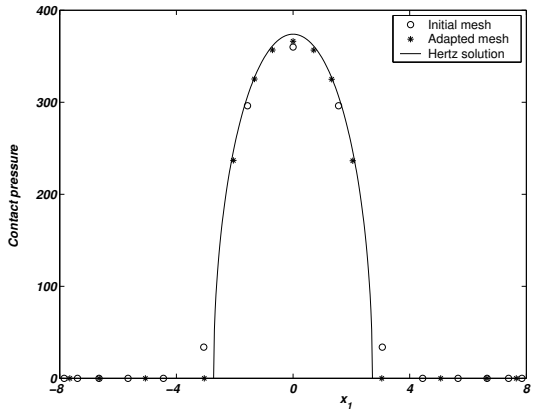

Fig. 10. Hertz test: Comparison of contact pressures.

3.4.4. A disc test

We present here a test inspired by the contact of a car wheel on a rigid obstacle standing for a road. The tire is idealized by an elastic disc Ω of radius 0.5. The obstacle is materialized by the line $x_2 = 0$. Elastic properties are given by

$$E = 10^7, \quad \nu = 0.45.$$

Finally, the "wheel" is assumed to be submitted to a vertical displacement at its centre equal to $u_2 = -0.05$. This singular condition ideally models the connection between the wheel and other parts of the vehicle.

Figures 11 and 12 show respectively the initial and adapted mesh of the reference configuration. Clearly, the mesh concentrates around the centre, where a singularity occurs due to the prescribed vertical displacement. In addition, as has been expected, a refinement occurs in the contact region as well as around the singularity that occurs at the disc centre. We can also note that the mesh symmetry around the axis $x_1 = 0$ is almost perfectly retained. Further calculation with a nonsymmetric mesh gave poor results. Figure 13 shows a comparison of contact pressures at contact nodes. We have compared the solution obtained for the initial and adapted meshes (made of 1184 elements) and a reference solution obtained with a very fine mesh (the disc is partitioned into 200 sectors and 50 layers, yielding 39400 elements). This figure shows that, except for the maximal pressure point, the obtained adapted pressure is very close to the reference one and, as for the Hertz test, the result is more spectacular for contact detection. It is also noticeable that this result is obtained for a very coarse mesh.

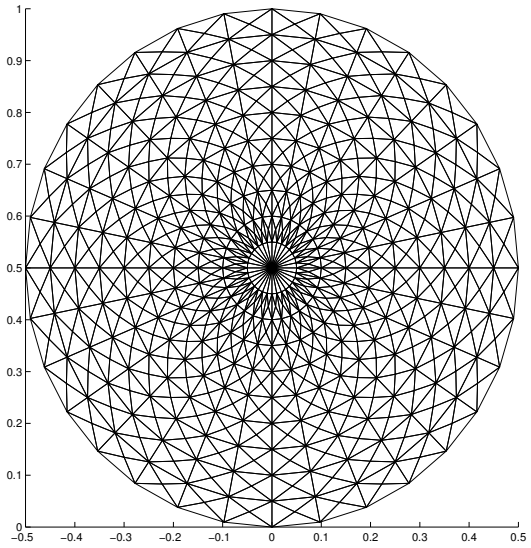

Fig. 11. Disc test: Initial mesh.

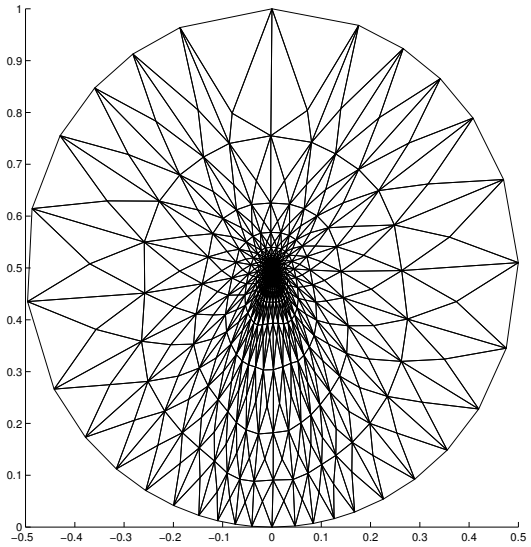

Fig. 12. Disc test: Adapted mesh.

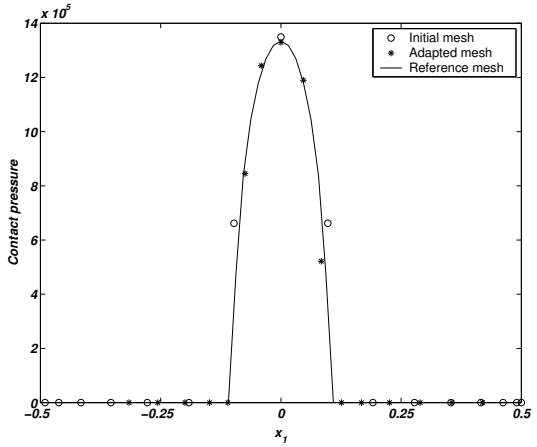

Fig. 13. Disc test: Comparison of contact pressures.

4. Conclusion

We have developed an r-adaptation mesh method that facilitates solving with sufficient accuracy a unilateral contact elasticity problem. The advantages of this method are its simplicity and its modularity, since it is completely independent of the solver (the method actually works for all elliptic linear and nonlinear problems). Its main drawback is its limitation to structured meshes (triangular and quadrilateral). We can conjecture that this is mainly due to the analogy of the finite element mesh with a spring network. A promising issue is the replacement of this analogy with the solution of a boundary value problem.

Acknowledgements

The authors are deeply indebted to C. Rahier and A. Rezgui from the MFP Michelin for fruitful discussions.

References

D'azevedo E.F. (1991): *Optimal triangular mesh generation by coordinate transformation*. — SIAM J. Sci. Stat. Comput., Vol. 12, No. 4, pp. 755–786.

D'azevedo E.F. and Simpson R.B. (1991): *On optimal triangular meshes for minimizing the gradient error*. — Üm. Math., Vol. 59, No. 4, pp. 321–348.

Fortin M. (1998): *Anisotropic mesh adaptation through hierarchical error estimators*. — SIAM J. Numer. Anal., Vol. 26, No. 4, pp. 788–811.

Habashi W.G., Fortin M., Yahia D.A.A., Boivin S., Bourgault Y., Dompierre J., Robichaud M.P., Tam A. and Vallet M.-G. (1996): *Anisotropic Mesh Optimization. Towards a Solver-Independent and Mesh-Independent CFD*. — Lecture Series in Computational Fluid Dynamics, Von Karman Institute for Fluid Dynamics.

Haslinger J., Neitaanmäki P. and Salmenjoki K. (1992): *On FE-grid relocation in solving unilateral boundary value problems by fem*. — Applics. Math., Vol. 37, No. 2, pp. 105–122.

Kikuchi N. and Oden J. (1988): *Contact Problems in Elasticity: A Study of Variational Inequalities and Finite Element Methods*. — Philadelphia, PA: SIAM.

Peraire J., Perió J. and Morgan K. (1992): *Adaptive remeshing for three-dimensional compressible flow computation*. — J. Comp. Phys., Vol. 103, No. 2, pp.269–285.

Tourigny Y. and Hülsemann F. (1998): *A new moving mesh algorithm for the finite element solution of variational problems*. — SIAM J. Numer. Anal., Vol. 35, No. 4, pp. 1416–1438.